THE ASTROPHYSICAL JOURNAL, 551:794–802, 2001 April 20


# THE CO $J = 2–1 / J = 1–0$ RATIO IN THE LARGE MAGELLANIC CLOUD

K. SORAI,[1,2] T. HASEGAWA,[1] R. S. BOOTH,[3] M. RUBIO,[4] J.-I. MORINO,[1,2] L. BRONFMAN,[4] T. HANDA,[1] M. HAYASHI,[5] L.-Å. NYMAN,[3,6] T. OKA,[7] S. SAKAMOTO,[2] M. SETA,[8] AND K. S. USUDA[1,5]

*Received 2000 January 4; accepted 2000 December 15*

## ABSTRACT

We observed 34 positions throughout the disk of the Large Magellanic Cloud in the CO $J = 2–1$ emission line with the Tokyo-Onsala-ESO-Calán 60 cm radio telescope. Comparing the spectra with those of the $J = 1–0$ line at the same angular resolution ($\simeq 9'$, or 130 pc at 50 kpc), we found that the CO $J = 2–1/J = 1–0$ intensity ratio ($R_{2-1/1-0}$) scatters in a range of 0.5–1.3. The luminosity ratio averaged for all observed points is $0.92 \pm 0.05$. The ratio $R_{2-1/1-0}$ is approximately unity ($0.95 \pm 0.06$) in 30 Dor, consistent with optically thick and thermalized emission, even in the southern part where massive star formation does not occur yet. This suggests that the high $R_{2-1/1-0}$ is not primarily due to the UV radiation from young stars but rather to the intrinsic nature of the molecular gas that is relatively dense ($\gtrsim 10^3$ cm$^{-3}$) and may be ready to form stars. In addition to a cloud-to-cloud difference of $R_{2-1/1-0}$, there exists a radial gradient of the ratio of $0.94 \pm 0.11$ in the inner region ($\lesssim 2$ kpc from the kinematic center) and $0.69 \pm 0.11$ in the outer region ($\gtrsim 2$ kpc from the center, excluding the 30 Doradus complex). The higher $R_{2-1/1-0}$ in the inner galaxy might be due to relatively higher gas densities within CO clumps in molecular clouds and/or higher external heating in that region.

*Subject headings:* galaxies: irregular — galaxies: ISM — ISM: clouds — ISM: molecules — Magellanic Clouds — radio lines: ISM

## 1. INTRODUCTION

Star formation influences, and is influenced by, the physical conditions in interstellar molecular gas in ways that are not well understood. The density, temperature, and velocity dispersion in the denser parts of molecular clouds can all play a role in regulating star formation, and massive stars, once formed, can alter the physical conditions in the clouds through UV radiation and stellar winds. Efforts have been made to deduce the physical conditions of molecular gas. The CO $J = 2–1/J = 1–0$ intensity ratio ($\equiv R_{2-1/1-0}$) has been used as one of the probes of physical conditions of molecular gas in local clouds and in the Galactic plane (see, e.g., Sakamoto et al. 1994, 1995; Oka et al. 1996). Previous observations have shown that it varies on a global scale in our Galaxy: there is a radial gradient of the $R_{2-1/1-0}$ ratio (Handa et al. 1993; Sakamoto et al. 1995), and $R_{2-1/1-0}$ is higher in the spiral arms (Sakamoto et al. 1997).

It is instructive to compare the global properties of molecular gas in other galaxies with those in our Galaxy. The Large Magellanic Cloud (LMC) is the nearest (50 kpc; Westerlund 1990) galaxy and one of the best laboratories for such a comparison. The LMC is characterized by low metallicity in the interstellar matter and ongoing formation of massive stars in clusters.

Extensive observations of the LMC have been made by Cohen et al. (1988), Garay et al. (1993), Israel et al. (1993), and Fukui et al. (1999) in CO $J = 1–0$ emission and by Israel et al. (1986) in CO $J = 2–1$ emission. Chin et al. (1996, 1997) have observed various molecular species in some clouds in the LMC. The Swedish ESO Submillimeter Telescope (SEST) Key Program has made a CO survey of the LMC (Israel et al. 1993; Kutner et al. 1997; Johansson et al. 1998) as well as of the Small Magellanic Cloud (SMC; see, e.g., Israel et al. 1993; Rubio, Lequeux, & Boulanger 1993; Lequeux et al. 1994). These observations have revealed that the CO emission is concentrated in a huge complex of molecular clouds associated with 30 Doradus. In the other regions, including that near the kinematic center, the emission is confined to small clouds with a small surface filling factor. The integrated CO $J = 1–0$ intensities of clouds in the LMC are at least 3 times weaker than those of comparable clouds in the Galactic disk (Israel et al. 1993; Kutner et al. 1997). This may be primarily because the CO-to-$H_2$ conversion factor in the LMC is a few times to an order of magnitude larger than that in the Galaxy (see, e.g., Cohen et al. 1988; Israel 1997; Fukui et al. 1999); the higher value may be due to the lower metallicity (see, e.g., Maloney & Black 1988; Elmegreen 1989; Sakamoto 1996). In the LMC a stronger UV radiation field is expected than in our Galaxy because of the lower metallicity and more active star formation, which leads to a higher gas-to-dust ratio. The stronger UV radiation field may cause a difference between the physical conditions of molecular clouds in the LMC and clouds in our Galaxy.

In this paper, we present results of the CO $J = 2–1$ observations of 34 positions throughout the disk of the LMC with the Tokyo-Onsala-ESO-Calán 60 cm CO survey telescope. Because the telescope was designed to have the same

[1] Institute of Astronomy, University of Tokyo, Mitaka, Tokyo 181-0015, Japan.
[2] Nobeyama Radio Observatory, National Astronomical Observatory, Minamimaki, Minamisaku, Nagano 384-1305, Japan.
[3] Onsala Space Observatory, Chalmers University of Technology, S-439 92 Onsala, Sweden.
[4] Departamento de Astronomía Universidad de Chile, Casilla 36-D, Santiago, Chile.
[5] Subaru Telescope, 650 North Aóhoku Place, Hilo, HI 96720.
[6] European Southern Observatory, Casilla 19001, Santiago 19, Chile.
[7] Department of Physics, University of Tokyo, Bunkyo, Tokyo 113-8654, Japan.
[8] Communications Research Laboratory, Koganei, Tokyo 184-8795, Japan.

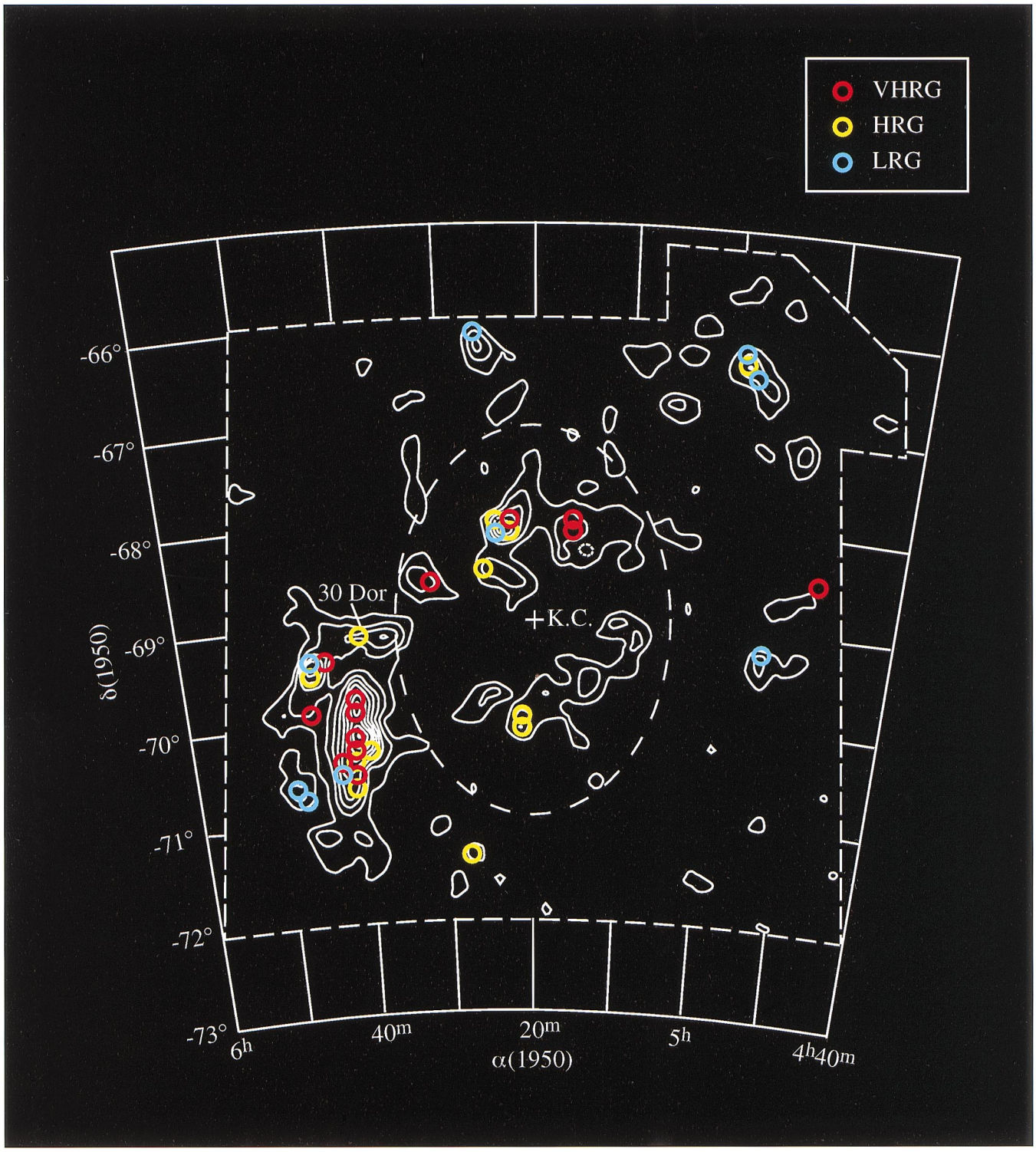


FIG. 1.—Observed positions are shown by beam-sized circles overlaid on the integrated intensity map of the CO $J = 1–0$ emission of Cohen et al. (1988). Each point is colored by the value of the intensity ratio between CO $J = 2–1$ and CO $J = 1–0$: very high ratio gas (VHRG: $R_{2-1/1-0} > 1.0$) is red, high-ratio gas (HRG: $0.7 \leq R_{2-1/1-0} \leq 1.0$) is yellow, and low-ratio gas (LRG: $R_{2-1/1-0} < 0.7$) is blue. The kinematic center (K.C.) is presented as a cross ($\alpha_{1950} = 5^h20^m$, $\delta_{1950} = -69°00'$; de Vaucouleurs & Freeman 1973). The ellipse (*dashed line*) corresponds to a circle with a radius of 2 kpc from the kinematic center using a distance of 50 kpc (Westerlund 1990), position angle of the line of node of 180° (Alvarez et al. 1987), and the inclination of the disk of 45°(Westerlund 1990).

beam width ($\simeq 9'$) as those of the 1.2 m telescopes used in CO $J = 1–0$ surveys of our Galaxy (see, e.g., Dame et al. 1987; Bronfman et al. 1988), the LMC (Cohen et al. 1988), and the SMC (Rubio et al. 1991), we could compare precisely the line intensities in both transitions. We investigate the global physical conditions of molecular gas in the LMC by means of the CO $J = 2–1/J = 1–0$ intensity ratios and compare them with those obtained in our Galaxy.

## 2. OBSERVATIONS

CO $J = 2$–1 line observations of the LMC were made with the Tokyo-Onsala-ESO-Calán 60 cm CO survey telescope (Very Small Telescope 2 [VST2]) at La Silla, Chile in 1996 August and September. The telescope has the same design as the Tokyo-NRO 60 cm CO survey telescope (VST1), which has been in operation at Nobeyama, Japan (Sakamoto et al. 1995). These telescopes were designed to have the same beam size in the CO $J = 2$–1 line as the CfA 1.2 m telescope does in the CO $J = 1$–0 line. By scanning the limbs of the sun, the half-power beam width (HPBW) of VST2 was measured to be $9'.2 \pm 0'.2$ at 230 GHz, corresponding to 130 pc at 50 kpc, the adopted distance of the LMC. The main-beam efficiency was $\eta_{\rm mb} = 0.91 \pm 0.03$. The receiver front end was a Shottky barrier diode mixer with a quasi-optical single sideband filter. The system noise temperature was 1000–1200 K at 230 GHz. For the back end, we used an acousto-optical spectrometer with a bandwidth of 1 GHz and a frequency resolution of 1.56 MHz, corresponding to 2.0 km s$^{-1}$ at 230 GHz.

We focused our observations on regions with relatively intense CO emission. We selected 34 positions guided by the original 1.2 m survey data of Cohen et al. (1988) before smoothing to 12′ resolution, with the antenna temperature, $T_a^*$, brighter than 0.1 K in CO $J = 1$–0, taking into consideration the noise in each spectrum. The only exception was the position at 30 Dor ($\alpha_{1950} = 5^{\rm h}39^{\rm m}39^{\rm s}$, $\delta_{1950} = -69°07'30''$), where the peak antenna temperature was 0.08 K in CO $J = 1$–0. The observed positions are shown by beam-sized circles in Figure 1, superposed on the CO $J = 1$–0 intensity contours. A few observed positions do not lie on the CO $J = 1$–0 peaks in Figure 1, which is an integrated intensity map smoothed to 12′ resolution, probably because our criteria were based on the peak antenna temperature before smoothing, not on the integrated intensity. All data were taken by position switching against off positions typically a few degrees away in azimuth. The integration time for each point was 50–70 minutes on source, resulting in a typical rms noise temperature of 30 mK in the main-beam brightness temperature, $T_{\rm mb}$.

## 3. RESULTS

CO $J = 2$–1 emission was detected at all 34 positions. Figure 2 compares three typical CO $J = 2$–1 profiles with the corresponding $J = 1$–0 profiles. The $J = 1$–0 spectra used throughout this paper are the original 8′.8 resolution data taken from Cohen et al. (1988). Their $T_a^*$ was then scaled to $T_{\rm mb}$, considering the main-beam efficiency of 0.82 (Bronfman et al. 1988). Note that there is clear variation of the intensity ratio from one position to another, although the line central velocity, velocity width, and the line shape are similar in the two transitions.

Table 1 lists the integrated intensities of the CO $J = 2$–1 and $J = 1$–0 emission as well as other line parameters. To avoid an additional error due to ambiguity of the baseline level, we determined the velocity integration ranges common to both transitions by inspection of the individual spectra. The range of integration is shown in Table 1 as minimum ($V_{\rm min}$) and maximum ($V_{\rm max}$) velocities. The integrated intensity of the $J = 1$–0 line is typically more than 1 K km s$^{-1}$. This value corresponds to a mass of $3.5 \times 10^5$ $M_\odot$ within the beam if we adopt the CO-to-$H_2$ conversion factor of $1.7 \times 10^{21}$ cm$^{-2}$ (K km s$^{-1}$)$^{-1}$ in the LMC

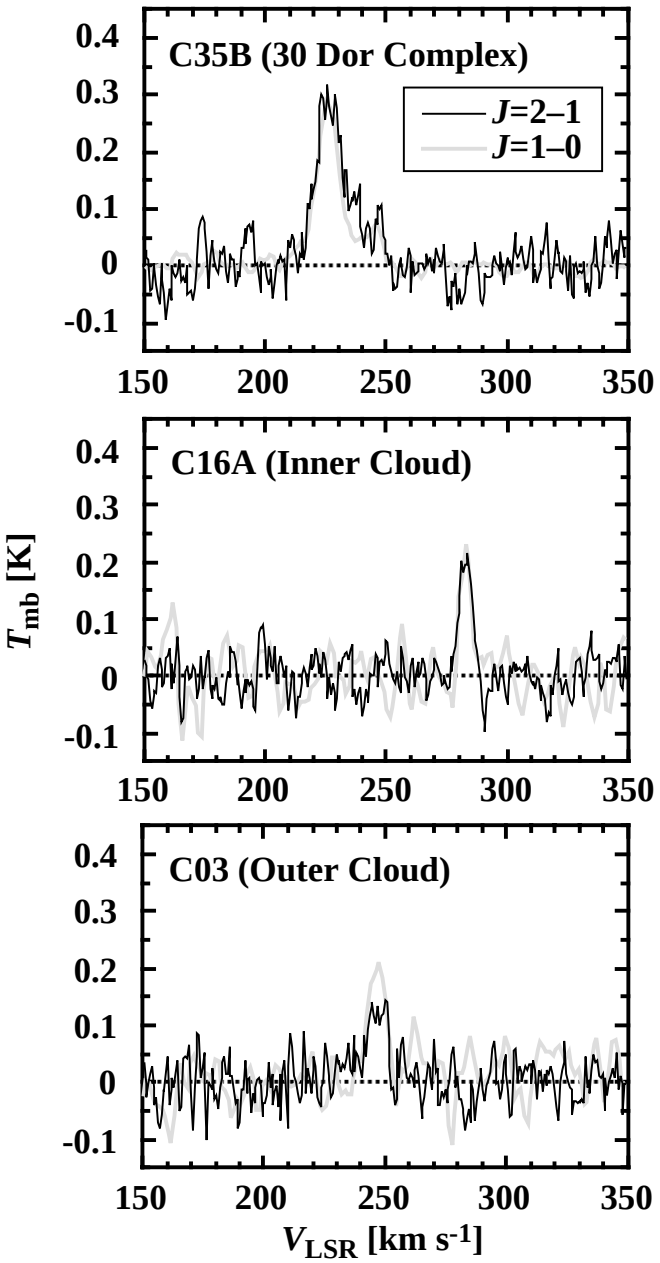


FIG. 2.—Typical profiles of CO $J = 2$–1 (*light lines*) and CO $J = 1$–0 (*heavy gray lines*). Horizontal axes are the velocities with respect to the local standard of rest (LSR), and the vertical ones are the main-beam brightness temperatures. The top panel shows the cloud in the 30 Dor complex, the middle one presents a cloud in the inner region, and the bottom one in the outer region of the LMC.

(Cohen et al. 1988), which is about 11 times larger than the Galactic value [$1.56 \times 10^{20}$ cm$^{-2}$ (K km s$^{-1}$)$^{-1}$; Hunter et al. 1997]. This implies that almost all of our observed points contain the mass of a giant molecular cloud.

The CO $J = 2$–1/$J = 1$–0 integrated intensity ratio ($\equiv R_{2-1/1-0}$) is indicated by the color of the circles in Figure 1. We also list $R_{2-1/1-0}$ at each observed point in Table 1. The ratio $R_{2-1/1-0}$ scatters in a range of 0.5–1.3, similar to that observed in our Galaxy. The luminosity-weighted average of $R_{2-1/1-0}$ for all points is $0.92 \pm 0.05$, which is higher than the ratio in the Galactic disk ($R_{2-1/1-0} = 0.66$ averaged over $20° \le l \le 60°$: Sakamoto et al. 1995; $R_{2-1/1-0} = 0.75$

TABLE 1

LINE PARAMETERS FOR OBSERVED POSITIONS

| Point[a] | $\alpha_{1950}$ | $\delta_{1950}$ | $\Delta V$[b] (km s$^{-1}$) | ($V_{min}$, $V_{max}$)[c] (km s$^{-1}$) | $\int T_{mb\,CO\,J=2-1}\,dV$ (K km s$^{-1}$) | $\int T_{mb\,CO\,J=1-0}\,dV$ (K km s$^{-1}$) | $R_{2-1/1-0}$ |
|---|---|---|---|---|---|---|---|
| **30 Doradus Complex Clouds** | | | | | | | |
| 30 Dor | 5 39 39 | −69 07 30 | 23.9 | (240, 280) | 1.37 ± 0.35 | 1.63 ± 0.41 | 0.84 ± 0.30 |
| C33A[d] | 5 40 13 | −69 45 00 | 11.0 | (225, 247) | 4.76 ± 0.30 | 3.92 ± 0.26 | 1.22 ± 0.11 |
| C33B | 5 40 21 | −69 52 30 | 10.8 | (224, 249) | 5.37 ± 0.33 | 5.22 ± 0.29 | 1.03 ± 0.09 |
| C33 total | | | | | 10.14 ± 0.45 | 9.14 ± 0.39 | 1.11 ± 0.07 |
| C35A | 5 40 35 | −70 07 30 | 13.1 | (218, 250) | 4.77 ± 0.47 | 4.44 ± 0.86 | 1.07 ± 0.23 |
| C35B | 5 40 43 | −70 15 00 | 13.6 | (217, 252) | 4.87 ± 0.51 | 3.85 ± 0.92 | 1.26 ± 0.33 |
| C35C | 5 40 51 | −70 22 30 | 8.0 | (220, 248) | 2.86 ± 0.49 | 2.89 ± 0.78 | 0.99 ± 0.32 |
| C35D | 5 39 14 | −70 15 00 | 25.5 | (218, 248) | 2.84 ± 0.57 | 3.15 ± 0.82 | 0.90 ± 0.30 |
| C35E | 5 42 20 | −70 22 30 | 12.0 | (220, 240) | 2.43 ± 0.48 | 2.34 ± 0.62 | 1.04 ± 0.34 |
| C35F | 5 42 28 | −70 30 00 | 7.4 | (222, 238) | 1.33 ± 0.23 | 2.20 ± 0.53 | 0.61 ± 0.18 |
| C35 total | | | | | 19.10 ± 1.15 | 18.88 ± 1.89 | 1.01 ± 0.12 |
| C36A | 5 40 58 | −70 30 00 | 9.4 | (222, 236) | 2.19 ± 0.26 | 1.98 ± 0.49 | 1.11 ± 0.30 |
| C36B | 5 41 06 | −70 37 30 | 12.5 | (217, 240) | 2.03 ± 0.45 | 2.20 ± 0.68 | 0.92 ± 0.35 |
| C36 total | | | | | 4.22 ± 0.52 | 4.18 ± 0.84 | 1.01 ± 0.24 |
| C37A | 5 45 33 | −69 22 30 | 10.5 | (220, 240) | 2.67 ± 0.39 | 4.30 ± 0.62 | 0.62 ± 0.13 |
| C37B | 5 45 42 | −69 30 00 | 8.1 | (222, 235) | 1.65 ± 0.30 | 2.33 ± 0.46 | 0.71 ± 0.19 |
| C37C | 5 44 08 | −69 22 30 | 15.4 | (225, 245) | 2.60 ± 0.49 | 2.48 ± 0.62 | 1.05 ± 0.33 |
| C37 total | | | | | 6.93 ± 0.69 | 9.12 ± 0.99 | 0.76 ± 0.11 |
| C39 | 5 46 09 | −69 52 30 | 26.9 | (220, 250) | 2.19 ± 0.48 | 1.73 ± 0.82 | 1.26 ± 0.66 |
| C40A | 5 47 18 | −70 45 00 | 8.1 | (210, 225) | 1.03 ± 0.23 | 1.72 ± 0.51 | 0.60 ± 0.22 |
| C40B | 5 48 38 | −70 37 30 | 8.5 | (210, 225) | 0.88 ± 0.28 | 1.64 ± 0.51 | 0.54 ± 0.24 |
| C40 total | | | | | 1.91 ± 0.36 | 3.35 ± 0.72 | 0.57 ± 0.16 |
| **Inner Clouds** | | | | | | | |
| C16A | 5 15 58 | −68 07 30 | 7.2 | (277, 288) | 1.35 ± 0.23 | 1.21 ± 0.41 | 1.11 ± 0.42 |
| C16B | 5 16 00 | −68 00 00 | 6.9 | (278, 290) | 1.19 ± 0.22 | 0.90 ± 0.44 | 1.32 ± 0.69 |
| C16 total | | | | | 2.53 ± 0.31 | 2.11 ± 0.60 | 1.20 ± 0.37 |
| C18A | 5 21 28 | −70 07 30 | 7.6 | (235, 245) | 1.23 ± 0.26 | 1.64 ± 0.39 | 0.75 ± 0.24 |
| C18B | 5 21 28 | −70 00 00 | 6.0 | (235, 247) | 1.40 ± 0.28 | 1.50 ± 0.44 | 0.93 ± 0.33 |
| C18 total | | | | | 2.63 ± 0.38 | 3.14 ± 0.59 | 0.83 ± 0.20 |
| C19A | 5 24 02 | −68 07 30 | 14.1 | (270, 285) | 1.42 ± 0.33 | 2.52 ± 0.51 | 0.56 ± 0.17 |
| C19B | 5 24 00 | −68 00 00 | 10.1 | (270, 287) | 1.90 ± 0.34 | 2.16 ± 0.55 | 0.88 ± 0.28 |
| C19C[e] | 5 22 41 | −68 07 30 | 14.0 | (272, 288) | 1.95 ± 0.37 | 2.29 ± 0.53 | 0.85 ± 0.26 |
| C19D[e] | 5 22 40 | −68 00 00 | 13.2 | (270, 290) | 2.67 ± 0.35 | 2.30 ± 0.52 | 1.16 ± 0.35 |
| C19 total | | | | | 7.95 ± 0.70 | 9.27 ± 1.11 | 0.86 ± 0.13 |
| C20 | 5 25 27 | −68 30 00 | 11.6 | (254, 273) | 1.51 ± 0.43 | 1.59 ± 0.60 | 0.95 ± 0.45 |
| C27 | 5 30 58 | −68 37 30 | 7.7 | (240, 270) | 1.78 ± 0.54 | 1.37 ± 0.82 | 1.30 ± 0.88 |
| **Outer Clouds** | | | | | | | |
| C02 | 4 49 59 | −68 30 00 | 5.9 | (245, 253) | 1.14 ± 0.17 | 0.95 ± 0.34 | 1.20 ± 0.46 |
| C03[f] | 4 54 36 | −69 15 00 | 10.3 | (240, 250) | 1.12 ± 0.24 | 1.65 ± 0.39 | 0.68 ± 0.22 |
| C06A | 4 58 54 | −66 15 00 | 3.9 | (273, 280) | 0.25 ± 0.20 | 0.88 ± 0.31 | 0.29 ± 0.25 |
| C06B | 4 58 47 | −66 22 30 | 10.1 | (272, 285) | 1.12 ± 0.32 | 1.14 ± 0.46 | 0.98 ± 0.49 |
| C06C[g] | 4 57 26 | −66 30 00 | 16.1 | (273, 290) | 0.87 ± 0.33 | 1.60 ± 0.55 | 0.54 ± 0.28 |
| C06 total | | | | | 2.24 ± 0.51 | 3.62 ± 0.78 | 0.62 ± 0.19 |
| C23[h] | 5 26 11 | −66 07 30 | 4.9 | (280, 290) | 0.70 ± 0.19 | 1.45 ± 0.39 | 0.48 ± 0.18 |

TABLE 1—*Continued*

| Point[a] | $\alpha_{1950}$ | $\delta_{1950}$ | $\Delta V^b$ (km s$^{-1}$) | $(V_{min}, V_{max})^c$ (km s$^{-1}$) | $\int T_{mb\,CO\,J=2-1}\,dV$ (K km s$^{-1}$) | $\int T_{mb\,CO\,J=1-0}\,dV$ (K km s$^{-1}$) | $R_{2-1/1-0}$ |
|---|---|---|---|---|---|---|---|
| C24..... | 5 27 50 | −71 22 30 | 6.1 | (222, 231) | 1.24 ± 0.17 | 1.64 ± 0.36 | 0.76 ± 0.20 |

NOTE.—Units of right ascension are hours, minutes, and seconds, and units of declination are degrees, arcminutes, and arcseconds.

[a] The positions are named after the cloud number in Table 1 of Cohen et al. 1988. When we observed more than two positions, capital letters are added: for example, the first and the second positions in the cloud number 19 are C19A and C19B, respectively.

[b] Full width at half-maximum of a spectrum.

[c] Minimum ($V_{min}$) and maximum ($V_{max}$) velocities for range of integration.

[d] Associated with H II region N159.

[e] Associated with H II region N44.

[f] Associated with H II region N83.

[g] Associated with H II region N11.

[h] Associated with supernova remnant SNR 0525−66.1 (N49).

at $R = 4$ kpc: Sakamoto et al. 1997). Although our observed points contain only 12% of the total molecular gas mass observed by Cohen et al. (1988), our results may reflect the general properties of molecular gas in the LMC since we found no clear correlation between the $R_{2-1/1-0}$ and the $J = 1$–0 line intensity in this galaxy.

The averaged value of $R_{2-1/1-0} \approx 0.9$ in the LMC implies that the molecular gas density $[n(H_2)]$ is higher than $\approx 10^3$ cm$^{-3}$ and the kinetic temperature ($T_k$) is higher than 10 K, according to a simple large velocity gradient (LVG) model (see, e.g., Sakamoto et al. 1994; Oka et al. 1998). Here we assume the relative abundance of CO to molecular hydrogen per unit velocity gradient $X_{CO}/(dV/dr)$ of $1 \times 10^{-6}$ (km s$^{-1}$ pc$^{-1}$)$^{-1}$, which is about 10 times smaller than that often applied for Galactic giant molecular clouds; the assumed value does not influence the derived density very much. In the case of our Galaxy, the value of $R_{2-1/1-0} \approx$ 0.6–0.8 corresponds to a density of $\approx 10^2$ cm$^{-3}$.

A closer point-by-point comparison is possible with our well-calibrated set of CO $J = 2$–1 and $J = 1$–0 data. Based on the CO distribution in the $J = 1$–0 map of Cohen et al. (1988), we tentatively classified the observed positions into three categories: the 30 Doradus complex, the inner region, and the outer region. The separation of the latter two is rather arbitrary, but we note that some molecular clouds are located in a ringlike distribution at 1 kpc from the kinematic center ($\alpha_{1950} = 5^h20^m$, $\delta_{1950} = -69°00'$; de Vaucouleurs & Freeman 1973). Beyond this radius there is a gap in the molecular cloud distribution near 2 kpc, and other molecular clouds are located $\gtrsim 3$ kpc from the center. With this spatial distribution in mind, we classified the clouds within 2 kpc from the kinematic center as "inner clouds" and ones farther out as "outer clouds." Here we adopt an inclination of the disk $i = 45°$ (Westerlund 1990) and a position angle of the line of node $\theta = 180°$ (Alvarez, Aparici, & May 1987) in order to calculate the radial distance from the kinematic center.

The averaged values of $R_{2-1/1-0}$ in these three categories are 0.95 ± 0.06 in the 30 Dor complex, 0.94 ± 0.11 in the inner clouds, and 0.69 ± 0.11 in the outer clouds. In Figure 1 the observed points are divided into three classes according to values of $R_{2-1/1-0}$: very high ratio gas (VHRG: $R_{2-1/1-0} > 1.0$), high-ratio gas (HRG: $0.7 \le R_{2-1/1-0} \le 1.0$), and low-ratio gas (LRG: $R_{2-1/1-0} < 0.7$) (Sakamoto et al. 1997). The spatial distribution of $R_{2-1/1-0}$ shows a trend: apart from the 30 Dor complex, the inner clouds tend to exhibit higher intensity ratios than the outer clouds. This tendency is also seen in Figure 3, which shows histograms of $R_{2-1/1-0}$ weighted by CO $J = 1$–0 luminosity for the three regions. In the inner region of the LMC, the fraction of VHRG and HRG to the total molecular gas is higher than that in the outer region. Table 2 shows the properties of molecular gas in each category, i.e., CO luminosities summed over all observed positions, $R_{2-1/1-0}$, line width, the [C II]/CO intensity ratio, and *IRAS* 60 $\mu$m flux density.

The ratio $R_{2-1/1-0}$ for inner clouds is not higher, because those clouds are systematically brighter in CO $J = 1$–0.

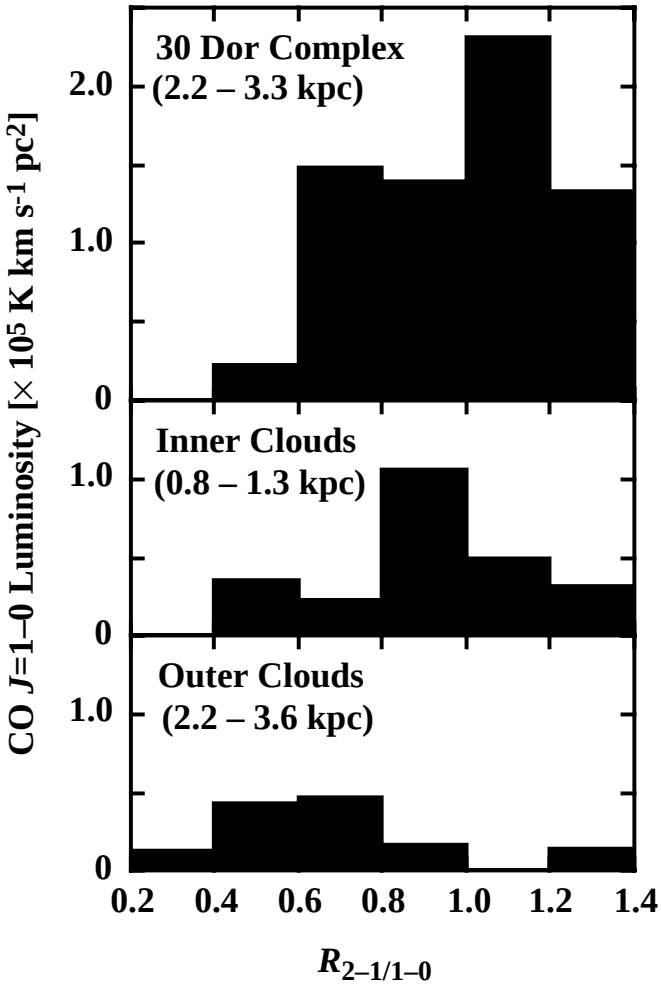


FIG. 3.—Histograms of $R_{2-1/1-0}$ weighted by CO $J = 1$–0 luminosity for the 30 Dor complex, inner clouds, and outer ones. The range of radial distance from the kinematic center is shown within parentheses.

TABLE 2

AVERAGED PROPERTIES OF CLOUDS

| Cloud | $\sum I_{CO\,J=2-1}$ ($10^5$ K km s$^{-1}$ pc$^2$) | $\sum I_{CO\,J=1-0}$ ($10^5$ K km s$^{-1}$ pc$^2$) | $R_{2-1/1-0}$ | $\Delta V$[a] (km s$^{-1}$) | [C II]/CO | *IRAS* 60 $\mu$m ($10^3$ Jy) |
|---|---|---|---|---|---|---|
| 30 Doradus complex clouds..... | 6.45 ± 0.23 | 6.76 ± 0.37 | 0.95 ± 0.06 | 10.6 ± 2.5 | 5800 ± 200 | 9.66 ± 0.06 |
| Inner clouds..... | 2.31 ± 0.15 | 2.46 ± 0.24 | 0.94 ± 0.11 | 8.8 ± 2.6 | 8800 ± 600 | 2.09 ± 0.05 |
| Outer clouds ..... | 0.91 ± 0.09 | 1.31 ± 0.15 | 0.69 ± 0.11 | 6.2 ± 2.4 | 5400 ± 600 | 1.08 ± 0.04 |
| Total ..... | 9.66 ± 0.29 | 10.52 ± 0.46 | 0.92 ± 0.05 | 9.2 ± 2.9 | 6400 ± 200 | 12.83 ± 0.09 |

[a] Average of full widths at half-maximum of the CO $J = 2–1$ spectra. Spectra with multiple peaks were not used for this average.

Figure 4 compares the intensities of $J = 1–0$ and $J = 2–1$ lines for the inner and outer clouds separately. The $J = 2–1$ emission is relatively brighter in the inner clouds than in the outer ones even though the $J = 1–0$ emission is almost the same in both groups.

## 4. DISCUSSION

### 4.1. 100 pc–*Scale Variation of* $R_{2-1/1-0}$*: Relation to Star Formation Activity*

#### 4.1.1. *The 30 Dor Cloud Complex*

30 Dor is associated with a huge complex of molecular gas that is 2.4 kpc in total length and $6 \times 10^7\ M_\odot$ in total mass (Cohen et al. 1988). It is a violent star-forming region where large numbers of very massive stars have formed in a limited area. To the south of 30 Dor, two bright H II regions, N160 and N159, are found. Israel et al. (1996) noted that this array of H II regions exhibits an age sequence from 30 Dor to the south based on differences in physical conditions and star formation indices: the northern part has already experienced active star formation, and present-day star formation activity has a peak near N159 ($\delta_{1950} \approx -69°45'$). Star formation has not occurred in the southern part of our observed points at present. This region is thus suitable to test the impact of star formation activity on $R_{2-1/1-0}$.

To express this evolutionary sequence in a more quantitative way, we adopt the intensity ratio between the [C II] (Mochizuki et al. 1994) and CO $J = 1–0$ lines. Here the CO $J = 1–0$ data are convolved to 15′, the beam size of the [C II] observations. The [C II]/CO ratio is thought to gauge the degree of destruction of molecular clouds by UV radiation from young stars. Figure 5 shows the [C II]/CO intensity ratio and the CO $J = 2–1$ integrated intensity as

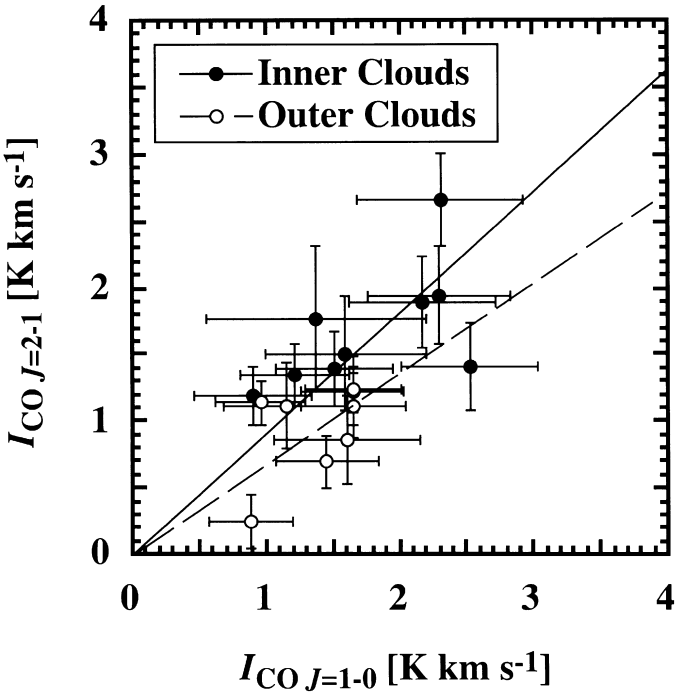


FIG. 4.—Correlation plot between CO $J = 1–0$ (*horizontal axis*) integrated intensity and that of $J = 2–1$ (*vertical axis*). Filled and open circles present the inner and outer clouds, respectively.

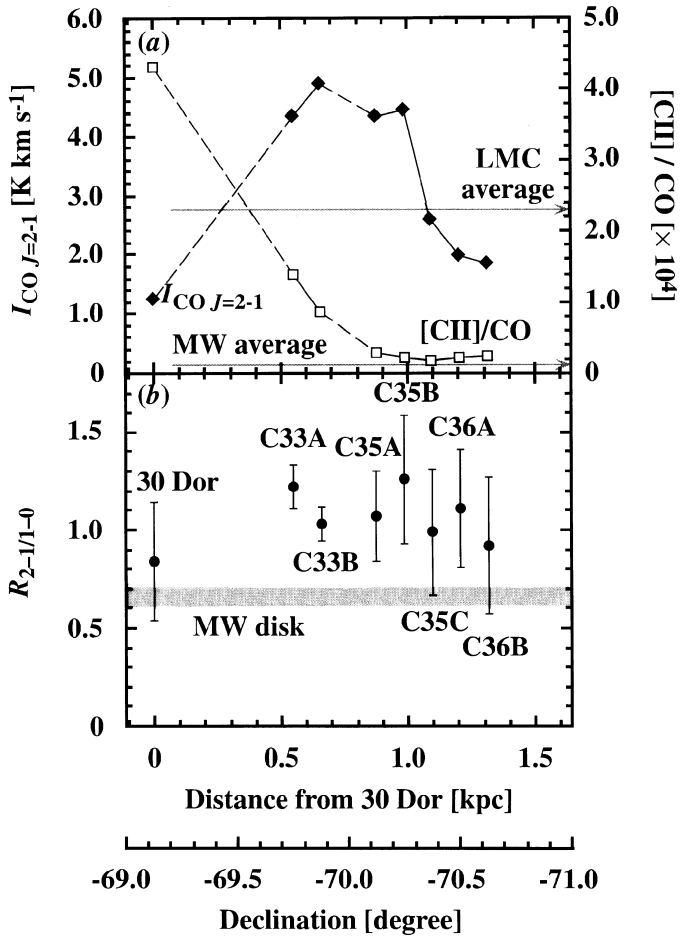


FIG. 5.—(*a*) Integrated intensity of CO $J = 2–1$ emission in K km s$^{-1}$ in the left-hand vertical axis (*filled diamonds*) and the intensity ratio between [C II] and CO $J = 1–0$ lines in the right-hand vertical axis times $10^4$ (*open squares*) as functions of a deprojected distance from 30 Dor (*horizontal axis, in kpc*). Dashed lines mean the neighboring observed points are apart from each other more than a beam size. The average values of the [C II]/CO ratio in the LMC (23,000) and our Galaxy (1300) (Mochizuki et al. 1994) are shown as gray lines. (*b*) Same as (*a*), but for the $R_{2-1/1-0}$ (*left-hand vertical axis*) intensity ratio. The typical value of $R_{2-1/1-0}$ in the disk of our Galaxy (0.6–0.7: Sakamoto et al. 1995) is shown by a gray band.

functions of the distance from 30 Dor. The evolutionary sequence is clearly expressed in this figure as a decrease of the [C II]/CO ratio, from 43,000 in 30 Dor to ~2000 in the southern region. The *IRAS* 60 $\mu$m surface brightness, which is another index of star formation, has a distribution similar to the [C II]/CO ratio.

It is clear from Figure 5 that $R_{2-1/1-0}$ is approximately unity even in the southern part of the 30 Dor complex, where star formation has not occurred yet and bright photodissociation regions (PDRs) are not found. This suggests that $R_{2-1/1-0}$ on a 100 pc scale is not enhanced because of star formation, but the ratio is intrinsically high in the entire 30 Dor complex, which corresponds to $n(H_2) >$ several $\times 10^3$ cm$^{-3}$ and may cause massive star formation in the future. The situation is different from the previous results on parsec scales in our Galaxy: in the Orion molecular cloud, VHRG is associated with H II regions, and HRG is preferably observed in the main ridge of the cloud, whereas LRG exists in the peripheral region of the cloud (Sakamoto et al. 1994). The high $R_{2-1/1-0}$ observed over the 30 Dor cloud complex suggests that it is ready to form massive stars.

#### 4.1.2. *Other Star-Forming Complexes*

The effects of individual star-forming regions and supernova remnants on $R_{2-1/1-0}$ can be evaluated by careful inspection of our data. Although there is a significant point-to-point difference of $R_{2-1/1-0}$, the one-to-one correspondence between $R_{2-1/1-0}$ and individual, vigorous star-forming regions is unclear. Some examples are described below. The H II region N44 (Henize 1956) is associated with the cloud C19, where $R_{2-1/1-0}$ is higher than 0.8 [$n(H_2) > 10^3$ cm$^{-3}$]. The [C II]/CO intensity ratio ($1.07 \times 10^4$), as well as *IRAS* 60 $\mu$m surface brightness ($> 7 \times 10^7$ Jy sr$^{-1}$), are highest among the disk clouds in the LMC. The clouds C06C and C03 are associated with the H II regions N11 and N83, respectively. The *IRAS* 60 $\mu$m surface brightness in these two clouds is very high among the disk clouds of the LMC, while the [C II]/CO intensity ratio is not particularly high ($6.26 \times 10^3$ and $4.34 \times 10^3$, respectively). The ratio $R_{2-1/1-0}$ is lower than 0.7 in both clouds. The CO $J = 2$–1 spectra of these clouds have multiple peaks, possibly because of disruption of the clouds by strong UV radiation from intense star formation. The cloud C23, containing the supernova remnant SNR 0525−66.1 (N49) (Mathewson et al. 1983; Banas et al. 1997), has an $R_{2-1/1-0}$ of $0.48 \pm 0.18$, which is not particularly high, in contrast to the case of the Galactic supernova remnant W44 (Seta et al. 1998). These results are consistent with the idea that the direct effects of individual H II regions and supernova remnants on $R_{2-1/1-0}$ are significant only within a few parsecs and do not control the properties of molecular gas averaged over 100 pc or more.

Figures 6*a* and 6*b* show correlation plots for the inner and outer clouds between $R_{2-1/1-0}$ and far-infrared indices of present-day massive star formation: the *IRAS* 60 $\mu$m surface brightness and the [C II]/CO $J = 1$–0 intensity ratio. There is no clear correlation between far-infrared indices of massive star formation and $R_{2-1/1-0}$. This correlation does not follow the one found for the nuclear regions of starburst galaxies (Aalto et al. 1995). The examples of individual clouds mentioned above show that the higher $R_{2-1/1-0}$ on 100 pc scales in the LMC does not result directly from massive star formation or supernova rem-

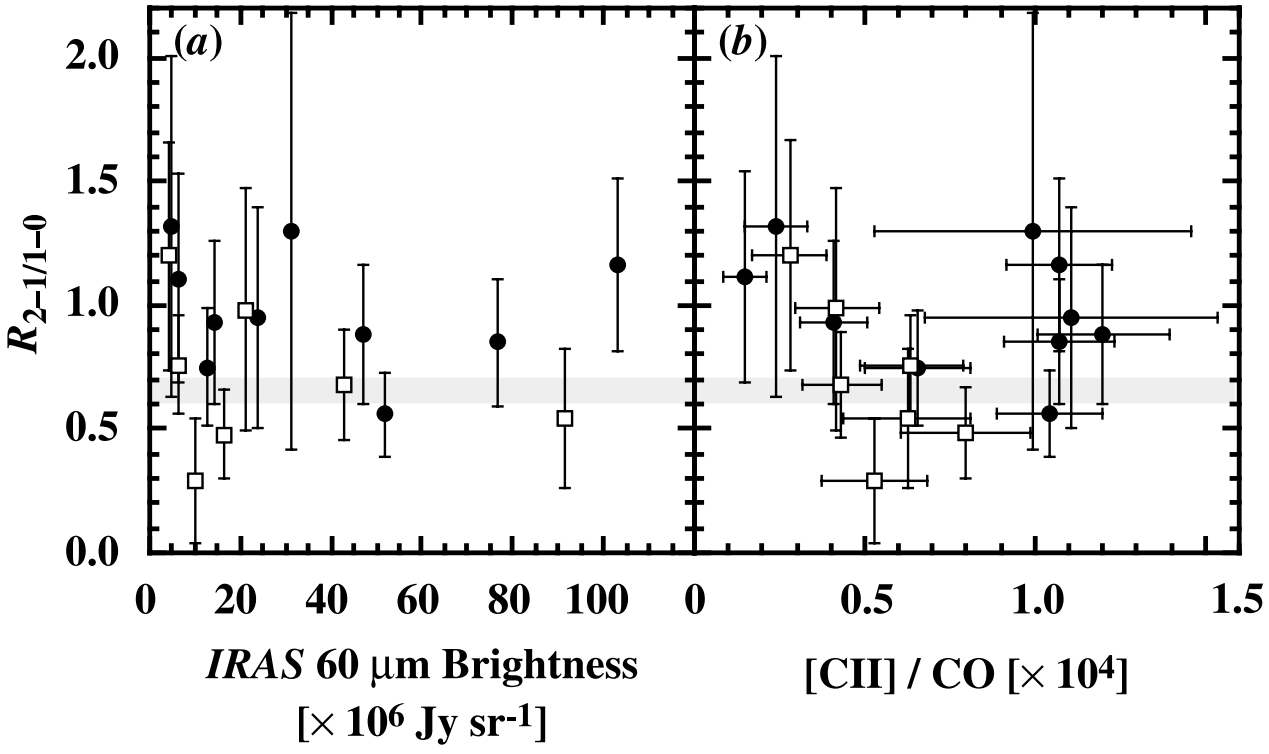


FIG. 6.—(*a*) Correlation between the CO intensity ratio and *IRAS* 60 $\mu$m surface brightness. Filled and open squares represent molecular clouds in the inner and outer regions, respectively. The typical value of $R_{2-1/1-0}$ in the disk of our Galaxy (0.6–0.7: Sakamoto et al. 1995) is shown by a gray band. (*b*) Same as (*a*), but for the correlation between the CO $J = 2$–1/$J = 1$–0 intensity ratio and the [C II]/CO ratio.

nants, although there is some relation on parsec scales, at least in the Galactic disk (Orion A and B: Sakamoto et al. 1994; W44: Seta et al. 1998; Rosette: Morino 1999).

### 4.2. *Kiloparsec-Scale Variation of* $R_{2-1/1-0}$

There seems to be a radial gradient in $R_{2-1/1-0}$ in the LMC: the luminosity-weighted mean value of $R_{2-1/1-0}$ is $0.94 \pm 0.11$ in the inner region of the LMC, which is higher than the value in the outer region ($0.69 \pm 0.11$), as shown in Table 2. According to simple LVG model analysis, this suggests that the inner clouds are both warmer ($T_k > 20$–$40$ K) and denser [$n(H_2) > 10^3$ cm$^{-3}$] than the outer clouds.

In our Galaxy, previous results in the first quadrant show a similar tendency: $R_{2-1/1-0}$ in the solar vicinity ($R \approx 8$–$9$ kpc) is lower than in the molecular ring at $R \approx 4$–$5$ kpc (Handa et al. 1993; Sakamoto et al. 1995; Sorai et al. 1996). The $R_{2-1/1-0}$ gradients shown in the LMC and our Galaxy may reflect a common mechanism that determines the average physical conditions of molecular gas in disk galaxies, although these two galaxies are different in morphology.

### 4.3. *Possible Causes of* $R_{2-1/1-0}$ *Enhancement*

The $R_{2-1/1-0}$ intensity ratio is higher in the 30 Dor cloud complex and the inner clouds than in the disk of our Galaxy, whereas the ratio in the outer clouds is comparable to that in the Galactic disk. Although there is a kiloparsec-scale variation of $R_{2-1/1-0}$ in the LMC, an enhancement of the ratio is not directly related to massive star formation on a 100 pc scale, as we have examined in § 4.2. Why is $R_{2-1/1-0}$ higher in the 30 Dor complex and in the inner clouds? What is the difference between the 30 Dor complex or the inner clouds and the outer ones? Or, more generally, what controls $R_{2-1/1-0}$?

There are four factors that might enhance $R_{2-1/1-0}$ from 0.6 to 1.0 in the LMC: (1) increase in temperature, (2) increase in $^{12}$CO opacity, (3) increase in density, and (4) a temperature gradient caused by external heating. We will examine these possibilities in the following subsections.

#### 4.3.1. *Temperature*

Increase in temperature seems less likely because molecular gas may be warmer than 10 K in the bright clouds sampled here, and in this case a large increase in gas temperature (up to $\gtrsim 35$ K) is needed to raise $R_{2-1/1-0}$ from 0.6 to 1.0. Higher spatial resolution observations with SEST showed a peak temperature of $T_{mb} \lesssim 6$ K on a 10 pc scale in the 30 Dor complex (Johansson et al. 1998). This suggests that a very small beam filling factor is needed to have a temperature higher than 35 K. There is no observational evidence to suggest that the bulk of the molecular gas in the inner clouds and the 30 Dor region has this high a temperature.

#### 4.3.2. $^{12}$CO *Opacity*

As for the second cause, increase of $^{12}$CO $J = 1–0$ opacity will be realized either by an increase of $^{12}$CO abundance ($X_{CO}$), by a decrease of velocity width per unit size ($dV/dr$), or by a decrease of the partition function due to low excitation temperature, and in any case significant variation is needed to produce the observed variation in $R_{2-1/1-0}$. There is, however, no evidence for significant variation of $dV/dr$. Significant increase of $^{12}$CO abundance toward the inner part is also unlikely in this dwarf galaxy. Decrease of the partition function may be in the opposite sense, or it may rather increase. Hence, it appears unlikely that an inward decrease of $^{12}$CO opacity is the cause of the $R_{2-1/1-0}$ gradient. Future large-scale observations in the $^{13}$CO line may test the validity of this argument.

#### 4.3.3. *Density and Clumpy Structure*

Increase in density may be a possible cause of $R_{2-1/1-0}$ enhancement. An LVG model shows that a range of $R_{2-1/1-0}$ from 0.6 to 1.0 is achieved when the gas density varies from $\approx 10^{2.5}$ to $\approx 10^3$ cm$^{-3}$. Actual clouds are composed of clumps, which have individual CO photospheres where the line optical depth integrated from the observer reaches $\sim 1$ (Sakamoto et al. 1994; Hasegawa 1996). In this case, a higher $R_{2-1/1-0}$ value suggests that the density within the photosphere is higher. In the LMC, interstellar UV radiation may penetrate the cloud more deeply in the LMC than in our Galaxy because of lower dust abundance. As a result, CO molecules may exist only in the inner, denser region of the clumps (Mochizuki et al. 1994). Because the density is generally higher toward the centers of the clumps, the average density within the CO photosphere is higher in the LMC than in our Galaxy. The higher $R_{2-1/1-0}$ observed in the inner clouds and the 30 Dor region in the LMC can be explained in this way, although this mechanism does not explain the lower $R_{2-1/1-0}$ in the outer clouds.

#### 4.3.4. *External Heating*

We cannot rule out the fourth possibility that enhanced external heating in the inner part of the LMC raises $R_{2-1/1-0}$ there. The stellar bar seen in optical images may cause a stronger interstellar radiation field in the inner region of the LMC. Indeed, the [C II]/CO intensity ratio is higher in the inner clouds than in the outer clouds. Intense external heating causes a positive temperature gradient near the CO photospheres of molecular clumps. Because of the larger opacity, the $J = 2–1$ transition "sees" a slightly outer, warmer surface relative to the $J = 1–0$ transition (Gierens, Stutzki, & Winnewisser 1992). This can enhance $R_{2-1/1-0}$ in the inner clouds. However, this mechanism cannot explain the case of the 30 Dor complex: [C II]/CO is much lower in the southern part of the 30 Dor complex, which is comparable to the value in our Galaxy.

In summary, we cannot identify a single way to explain the observed large-scale variation in $R_{2-1/1-0}$. An increase in the average density within CO photospheres can explain the higher $R_{2-1/1-0}$ in the LMC than in our Galaxy but cannot explain the difference between the inner and outer clouds. A temperature gradient at the cloud surface due to an intense external heating can explain the higher $R_{2-1/1-0}$ in the inner clouds than in the outer clouds, but the high ratio in the southern part of the 30 Dor complex is left unexplained. Higher resolution observations in both $^{12}$CO $J = 2–1$ and $^{13}$CO are needed to draw a definite answer.

## 5. CONCLUSIONS

We observed 34 points throughout the disk of the Large Magellanic Cloud in the CO $J = 2–1$ emission line. Through close comparison with the CO $J = 1–0$ data taken by Cohen et al. (1988) with the same beam width, we found the following:

1. The CO $J = 2–1/J = 1–0$ intensity ratio ($R_{2-1/1-0}$) scatters in a range of 0.5–1.3. The mean luminosity ratio for all observed points is $0.92 \pm 0.05$.

2. In addition to a point-to-point (i.e., cloud-to-cloud) difference of $R_{2-1/1-0}$, there exists a kiloparsec-scale variation of the ratio, which is $0.95 \pm 0.06$ in the 30 Doradus complex, $0.94 \pm 0.11$ within 2 kpc of the kinematic center, and $0.69 \pm 0.11$ in the outer part, excluding the 30 Doradus complex. The radial gradient of $R_{2-1/1-0}$, which is higher in the inner clouds, while lower in the outer clouds, is similar to the case in our Galaxy. A common mechanism may determine the average physical conditions of molecular gas, although these two galaxies are different in morphology.

3. In the 30 Doradus complex, $R_{2-1/1-0}$ is approximately unity even in the southern part, where massive star formation has not occurred yet. This suggests that the high $R_{2-1/1-0}$ is not primarily due to the effect of UV photons from young stars but is intrinsic to the molecular gas there. It is relatively dense ($\gtrsim 10^3$ cm$^{-3}$) and may be ready to initiate star formation.

4. An increase in the average density within clouds can explain the higher $R_{2-1/1-0}$ in the LMC than in our Galaxy but cannot explain the difference between the inner and outer clouds in the LMC. A temperature gradient at the cloud surface due to intense external heating can explain the higher $R_{2-1/1-0}$ in the inner clouds than in the outer clouds but cannot explain the high ratio in the southern part of the 30 Dor complex. We cannot identify a simple way to explain the observed large-scale variation in $R_{2-1/1-0}$. Further high-resolution observations in $^{12}$CO $J = 2$–1 as well as in $^{13}$CO are needed to test the above possibilities.

This work was made as a part of the Tokyo-Onsala-ESO-Calán Galactic CO Survey program under the collaboration of the radio astronomy group of the University of Tokyo, Onsala Space Observatory, European Southern Observatory, and the Department of Astronomy of the University of Chile. We express special thanks to Peter Shaver for his help in organizing the collaboration. We acknowledge Kenji Mochizuki for providing us with the [C II] data. We are indebted to the referee, T. M. Dame, for valuable comments that improved the paper greatly. The work was supported by the Ministry of Education, Science, Sports, and Culture, Grant-in-Aid for Scientific Research, 08404009 (T. H.), 09044058 (T. H.), and 10147202 (T. H.). L. B. acknowledges support by a Cátedra Presidencial en Ciencias and by Fondecyt Grant 8970017.

## REFERENCES

Aalto, S., Booth, R. S., Black, J. H., & Johansson, L. E. B. 1995, A&A, 300, 369
Alvarez, H., Aparici, J., & May, J. 1987, A&A, 176, 25
Banas, K. R., Hughes, J. P., Bronfman, L., & Nyman, L.-Å. 1997, ApJ, 480, 607
Bronfman, L., Cohen, R. S., Alvarez, H., May, J., & Thaddeus, P. 1988, ApJ, 324, 248
Chin, Y.-N., Henkel, C., Millar, T. J., Whiteoak, J. B., & Mauersberger, R. 1996, A&A, 312, L33
Chin, Y.-N., Henkel, C., Whiteoak, J. B., Millar, T. J., Hunt, M. R., & Lemme, C. 1997, A&A, 317, 548
Cohen, R. S., Dame, T. M., Garay, G., Montani, J., Rubio, M., & Thaddeus, P. 1988, ApJ, 331, L95
Dame, T. M., et al. 1987, ApJ, 322, 706
de Vaucouleurs, G., & Freeman, K. 1973, Vistas Astron., 14, 163
Elmegreen, B. G. 1989, ApJ, 338, 178
Fukui, Y., et al. 1999, PASJ, 51, 745
Garay, G., Rubio, M., Ramírez, S., Johansson, L. E. B., & Thaddeus, P. 1993, A&A, 274, 743
Gierens, K. M., Stutzki, J., & Winnewisser, G. 1992, A&A, 259, 271
Handa, T., Hasegawa, T., Hayashi, M., Sakamoto, S., Oka, T., & Dame, T. 1993, in AIP Conf. Proc. 278, Back to the Galaxy, ed. S. S. Holt & F. Verter (New York: AIP), 315
Hasegawa, T. 1996, in IAU Symp. 170, CO: Twenty-five Years of Millimeter-Wave Spectroscopy, ed. W. B. Latter, S. J. E. Radford, P. R. Jewell, J. G. Mangum, & J. Bally (Dordrecht: Kluwer), 39
Henize, K. G. 1956, ApJS, 2, 315
Hunter, S. D., et al. 1997, ApJ, 481, 205
Israel, F. P. 1997, A&A, 328, 471
Israel, F. P., de Graauw, Th., van de Stadt, H., & de Vries, C. P. 1986, ApJ, 303, 186
Israel, F. P., et al. 1993, A&A, 276, 25
Israel, F. P., Maloney, P. R., Geis, N., Herrmann, F., Madden, S. C., Poglitsch, A., & Stacey, G. J. 1996, ApJ, 465, 738
Johansson, L. E. B., et al. 1998, A&A, 331, 857
Kutner, M. L., et al. 1997, A&AS, 122, 255
Lequeux, J., Le Bourlot, J., Pineau des Forêts, G., Roueff, E., Boulanger, F., & Rubio, M. 1994, A&A, 292, 371
Maloney, P., & Black, J. H. 1988, ApJ, 325, 389
Mathewson, D. S., Ford, V. L., Dopita, M. A., Tuohy, I. R., Long, K. S., & Helfand, D. J. 1983, ApJS, 51, 345
Mochizuki, K., et al. 1994, ApJ, 430, L37
Morino, J. -I. 1999, Ph.D. thesis, Univ. Tokyo
Oka, T., Hasegawa, T., Handa, T., Hayashi, M., & Sakamoto, S. 1996, ApJ, 460, 334
Oka, T., Hasegawa, T., Hayashi, M., Handa, T., & Sakamoto, S. 1998, ApJ, 493, 730
Rubio, M., Garay, G., Montani, J., & Thaddeus, P. 1991, ApJ, 368, 173
Rubio, M., Lequeux, J., & Boulanger, F. 1993, A&A, 271, 9
Sakamoto, S. 1996, ApJ, 462, 215
Sakamoto, S., Hasegawa, T., Handa, T., Hayashi, M., & Oka, T. 1997, ApJ, 486, 276
Sakamoto, S., Hasegawa, T., Hayashi, M., Handa, T., & Oka, T. 1995, ApJS, 100, 125
Sakamoto, S., Hayashi, M., Hasegawa, T., Handa, T., & Oka, T. 1994, ApJ, 425, 641
Seta, M., et al. 1998, ApJ, 505, 286
Sorai, K., et al. 1996, in Ground-Based Astronomy in Asia, ed. N. Kaifu (Tokyo: National Astronomical Observatory), 115
Westerlund, B. E. 1990, Astron. Astrophys. Rev., 2, 29